

# Res6D: Projective Residual Regression for 6D Pose Estimation

Jianqiu Chen<sup>1\*</sup>   Mingshan Sun<sup>2\*</sup>   Ye Zheng<sup>3</sup>   Tianpeng Bao<sup>2</sup>   Zhenyu He<sup>1†</sup>  
 Donghai Li<sup>2</sup>   Guoqiang Jin<sup>2</sup>   Rui Zhao<sup>2</sup>   Liwei Wu<sup>2</sup>   Xiaoke Jiang<sup>4</sup>  
 Harbin Institute of Technology, Shenzhen<sup>1</sup>  
 SenseTime Research<sup>2</sup>  
 JD.com, Inc<sup>3</sup>  
 International Digital Economy Academy (IDEA)<sup>4</sup>

## Abstract

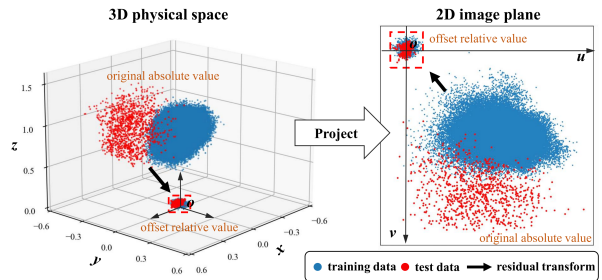
In RGB-D based 6D pose estimation, direct regression approaches can directly predict the 3D rotation and translation from RGB-D data, allowing for quick deployment and efficient inference. However, directly regressing the absolute translation of the pose suffers from diverse object translation distribution between the training and testing datasets, which is usually caused by the diversity of pose distribution of objects in 3D physical space. To this end, we generalize the pin-hole camera projection model to a **residual-based projection model** and propose the **projective residual regression (Res6D)** mechanism. Given a reference point for each object in an RGB-D image, Res6D not only reduces the distribution gap and shrinks the regression target to a small range by regressing the residual between the target and the reference point, but also aligns its output residual and its input to follow the projection equation between the 2D plane and 3D space. By plugging Res6D into the latest direct regression methods, we achieve state-of-the-art overall results on datasets including Occlusion LineMOD (ADD(S): 79.7%), LineMOD (ADD(S): 99.5%), and YCB-Video datasets (AUC of ADD(S): 95.4%).

## 1. Introduction

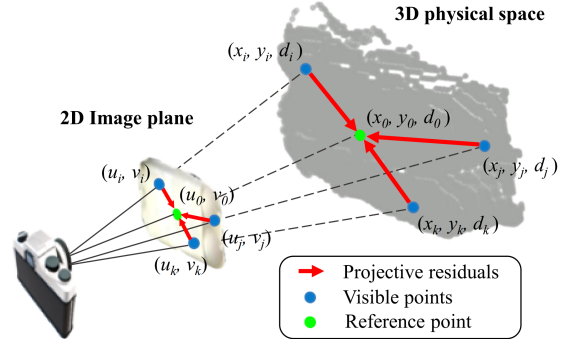
6D pose estimation has drawn widespread attention as the essential prerequisite of emerging applications, such as robotic manipulation, autonomous driving, and augmented reality [3, 8, 31]. Due to the reasonably priced RGB-D sensor, it has become a common practice to estimate 6D pose from RGB-D data, which has been significantly advanced in recent years with deep learning technologies, whether through direct and indirect regression methods. Indirect methods [11, 12, 27] usually predict an intermediate re-

\*These authors contributed equally to this work.

†Corresponding authors.



(a) Distribution of object translation ( $\mathbf{t}$ ) on Occlusion LineMOD: 1) distribution of absolute  $\mathbf{t}$  between training and testing data is diversely distributed in a wide range; 2) distribution of relative  $\mathbf{t}$  (after residual transformation) is much more compact).



(b) The proposed projective residuals in the pin-hole camera projection model. Red arrows are residuals from visible points to the reference point.

Figure 1. The translation distribution and proposed projective residuals.

sult first, then use the post-processing optimization algorithm, such as a least-squares fitting algorithm and iterative Perspective-n-Point (PnP) algorithms [9, 17, 19, 22, 24], to calculate the final result, whereas the direct methods [16, 18, 20, 25, 28, 29] predict the final 6D pose directly without post-processing, *i.e.*, in an end-to-end manner. However, directly regressing the absolute translation of the pose suf-

fers from diverse object translation distribution between the training and testing datasets. As shown in Fig. 1a, the object translation  $\mathbf{t}$  between training (blue dots) and testing (red dots) datasets in Occlusion LineMOD [1] are *diversely* distributed in a *wide* range. Due to the costly data collection and annotation in 6D pose estimation, diverse distribution between training and testing datasets inevitably severely restricts the model’s ability to generalize, which is quite common in practice.

Intuitively, a naive strategy to fix the aforementioned issue is to change the regression target  $\mathbf{t}$  to be the offset of the object’s translation to a given reference point, which is represented by 3D coordinates  $(x_0, y_0, d_0)$  in the 3D physics world. In this way, the reshaped regression target (residual of  $\mathbf{t}$  between the reference point and the absolute value) could reduce the domain gap and scatters in a small range, as shown in Fig. 1a. This 3D residual regression strategy converts the absolute value of the pose to a relative value, effectively reducing the distribution difference between the training set and the testing set. However, the fly in the ointment is the pose estimating network needs to find out the correspondence between the current input data and the CAD model, while using absolute 2D location encoding in the image plane to predict the relative position of the CAD model breaks this correspondence. Revisiting the pin-hole camera projection model:

$$\begin{bmatrix} u_i \\ v_i \\ 1 \end{bmatrix} = \frac{\mathbf{K}}{d_i} \begin{bmatrix} x_i \\ y_i \\ d_i \end{bmatrix} = \frac{\mathbf{K}}{d_i} \left( \mathbf{R} \times \begin{bmatrix} a_i \\ b_i \\ c_i \end{bmatrix} + \mathbf{t} \right) \quad (1)$$

a point  $(a_i, b_i, c_i)$  in the object coordinate system is first rotated and translated by rotation matrix  $\mathbf{R}$  and translation vector  $\mathbf{t}$  to the position  $(x_i, y_i, d_i)$  in the camera coordinate system, then it is projected to the pixel at  $(u_i, v_i)$  in the image plane through the intrinsic matrix  $\mathbf{K}$  of the camera. Directly applying the 3D residual regression strategy breaks this projection relationship, leading to two mismatches in Eq. (2) and Eq. (3). In Eq. (2), after subtracting the 3D reference point from a visible point inside the object, the first mismatching occurs between absolute UV  $(u_i, v_i)$  and the CAD model, which is an obstacle for the network to estimate the relation between input UV data and 6D pose. The second mismatching in Eq. (3) is from the absolute UV  $(u_i, v_i)$  and relative XYD  $(x_i - x_0, y_i - y_0, d_i - d_0)$ , making the network is hard to learn the correct camera intrinsic  $\mathbf{K}$ .

$$\begin{bmatrix} u_i \\ v_i \\ 1 \end{bmatrix} \neq \frac{\mathbf{K}}{d_i} \left( \mathbf{R} \times \begin{bmatrix} a_i \\ b_i \\ c_i \end{bmatrix} + \mathbf{t} \right) - \frac{\mathbf{K}}{d_0} \left( \mathbf{R} \times \begin{bmatrix} a_0 \\ b_0 \\ c_0 \end{bmatrix} + \mathbf{t} \right), \quad (2)$$

$$\begin{bmatrix} u_i \\ v_i \\ 1 \end{bmatrix} \neq \frac{\mathbf{K}}{(d_i - d_0)} \begin{bmatrix} x_i - x_0 \\ y_i - y_0 \\ d_i - d_0 \end{bmatrix} \quad (3)$$

To this end, we generalize the original pin-hole camera projection model Eq. (1) to the residual-based projection model Eq. (7) by considering the case of introducing residual regression and propose the projective residual regression (Res6D) mechanism. As shown in Fig. 1b, after selecting the 3D reference point  $(x_0, y_0, d_0)$  inside the object, Res6D first obtains its 2D reference point  $(u_0, v_0)$  based on the residual-based projection model, then replaces the absolute input information of all visible points in the object with the residual value of the reference point. Different from the naive 3D residual regression strategy that only considers the 3D physical space, Res6D adjusts the 2D and 3D coordinates simultaneously with a reference point  $(u_0, v_0, x_0, y_0, d_0)$ . Furthermore, Res6D reduces the distribution gap between the training and testing dataset, which can accelerate model convergence and reduce data dependencies. It only requires 10% of training data to reach the comparable performance of full training data. We also observe that Res6D can balance the translation and rotation part of the ADD loss function, which further improves the performance.

To summarize, our main contributions are:

- We uncover the issue of the object translation distribution between training and testing datasets in existing direct regression backbone methods, which limits the generalization ability of the model and the performance.
- We propose the projective residual regression (Res6D) mechanism by generalizing the original pin-hole camera projection model to a residual-based projection mode to solve the above issue, which narrows the gap of the translation distribution and improves the performance. Res6D can also reduce data requirements and balance the translation and rotation part of the ADD loss function.
- Extensive experimental results show that the proposed Res6D can effectively improve the performance of existing direct regression methods, and achieves state-of-the-art overall results.

## 2. Related work

We review the indirect and direct 6D pose estimation methods and different residual mechanisms in this section.

### 2.1. Indirect methods

Indirect methods first predict intermediate geometric information, and then exploit the projection constraints to estimate the 6D pose by optimization function. Recent methods [11, 12, 21] introduce the keypoints mechanism in 6D pose estimation and then estimate the 6D pose by a least-squares fitting algorithm. Different from the keypoints-

based methods, 2D-3D correspondence-based methods [9, 14, 17, 19, 22, 24] first establish the correspondence between 2D coordinates in the image plane and 3D coordinates in the object coordinate system by the neural network and then solve the 6D pose by a PnP or RANSAC algorithm. However, these indirect methods are only optimized in the first stage rather than the final pose regression, which is suboptimal compared with direct methods. Moreover, the optimization is time-consuming and heavy in practical applications.

## 2.2. Direct methods

To estimate 6D pose efficiently, recent approaches [16, 18, 20, 28, 29] directly regress the final 6D pose parameters instead of intermediate results. Densefusion [27] extract geometric and appearance information from RGB-D images individually and fuse them by a dense fusion network. Yet, the heterogeneous architecture is still heavy in practical applications. Uni6D series [16, 25] simplify the architecture by a single backbone. Uni6D [16] exposes the projection breakdown problem of processing depth image in the CNN framework and first leverages a single homogeneous backbone to process RGB-D data, introducing the extra UV data into input to preserve the projection constraint. In the following work uni6Dv2 [25], a two-step denoising approach is proposed to guide the network to learn the object-relevant feature and calibrate depth information. However, it is challenging to directly regress the absolute translation because the output space is theoretically infinite, especially when there is a distribution gap between the training and test dataset. To alleviate the aforementioned problem, ES6D [20] densely regresses offsets from visible points to the centroid point in 3D space. However, the mismatch between the input and output limits the accuracy of pose estimation.

## 2.3. Residual mechanisms

Deep residual is widely used in image recognition [10], which reformulate the layers as learning residual functions with reference to the layer inputs. [5–7, 23, 26] regress residual of the output between output of module and ground truth. Similarly, some 6D pose estimation methods [11, 12, 20] take a similar operation to regress the offsets of visible points and predefined 3D keypoints or 3D visible points. The above residual mechanisms compact output distribution and decrease the the difficulty of network convergence. However, it has a potential pitfall for the 6D pose estimation task: the mismatch correspondences between RGB-D and CAD model, which breaks the projection equation and severely limits the performance. Hence, we propose the Res6D in the 2D image plane and 3D space. Unlike the keypoint-based pose estimation method to regress the offset of visible points to keypoints, we regress the off-

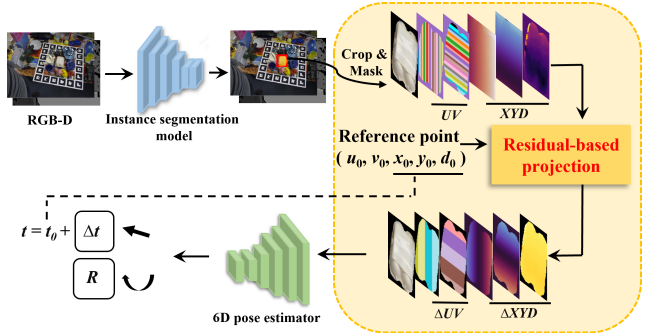


Figure 2. Overview of our proposed Res 6D pose estimation process. The absolute input is converted to offset by reference point, and the final translation  $t$  is calculated by adding the reference point position  $t_0$  with predicted offsets  $\Delta t$ .

set of the reference point to the centroid to predict the final pose directly. Mostly, we propose the residual-based projection model and overcome the mismatch problem.

## 3. Method

In this section, we first give an overview of our projective residual 6D pose estimation (Res6D) solution. Then present the residual-based projection and reference point, and finally, we analyze the balance of rotation and translation training losses after introducing the reference point.

### 3.1. Overview

We summarize our projective residual for 6D pose estimation in Fig. 2. Given an RGB-D input image, we first take an object instance segmentation model to predict the bounding box and mask of the target object and obtain the patch with absolute UV and XY data, which is cropped and masked by the results of the instance segmentation network. We then select a reference point inside the object and apply the proposed residual-based model on the patch to get relative input  $\Delta UV$ ,  $\Delta XYD$  from the reference point. Lastly, feeding the relative input into a 6D pose estimator to get the rotation and relative translation  $\Delta t$ , which can be thought of as regression from a reference point  $(x_0, y_0, d_0)$  to target translation  $t$ . The final translation result is the summary of the predicted relative one and  $(x_0, y_0, d_0)$ . Following residual-based projection, the pose estimation with reference point could be formulated as:

$$R, \Delta t = f(RGB, \Delta U, \Delta V, \Delta X, \Delta Y, \Delta D). \quad (4)$$

### 3.2. Residual-based projection

Given a visible point  $(u_i, v_i, x_i, y_i, d_i)$ , it should satisfy the following projection equation according to Eq. (1):

$$\begin{bmatrix} u_i \\ v_i \\ 1 \end{bmatrix} = \mathbf{K} \begin{bmatrix} \frac{x_i}{d_i} \\ \frac{y_i}{d_i} \\ 1 \end{bmatrix} = \mathbf{K} \left( \mathbf{R} \times \begin{bmatrix} \frac{a_i}{d_i} \\ \frac{b_i}{d_i} \\ \frac{c_i}{d_i} \end{bmatrix} + \frac{\mathbf{t}}{d_i} \right), \quad (5)$$

we set a reference point  $(u_0, v_0, x_0, y_0, d_0)$  (green dot in Fig. 1b) for it in both 2D image plane and 3D physical space, which satisfies the following projection model:

$$\begin{bmatrix} u_0 \\ v_0 \\ 1 \end{bmatrix} = \mathbf{K} \begin{bmatrix} \frac{x_0}{d_0} \\ \frac{y_0}{d_0} \\ 1 \end{bmatrix} = \mathbf{K} \left( \mathbf{R} \times \begin{bmatrix} \frac{a_0}{d_0} \\ \frac{b_0}{d_0} \\ \frac{c_0}{d_0} \end{bmatrix} + \frac{\mathbf{t} - \mathbf{t}_0 + \mathbf{t}_0}{d_0} \right), \quad (6)$$

where  $\mathbf{t}_0$  denotes the position  $(x_0, y_0, d_0)$  of the reference point in 3D space of camera coordinate system.

According to Eq. (5), both sides of the projection equation subtract the 2D coordinates  $(u_0, v_0)$  and 3D coordinates  $(x_0, y_0, d_0)$  respectively in Eq. (6). The projection constraint about a visible point  $(u_i, v_i, x_i, y_i, d_i)$  and the reference point is reformulated in relative value according to the reference point, which is denoted as residual-based projection model:

$$\begin{bmatrix} \Delta u \\ \Delta v \\ 0 \end{bmatrix} = \mathbf{K} \begin{bmatrix} \Delta x \\ \Delta y \\ 0 \end{bmatrix} = \mathbf{K} \left( \mathbf{R} \times \begin{bmatrix} \frac{a_i}{d_i} - \frac{a_0}{d_0} \\ \frac{b_i}{d_i} - \frac{b_0}{d_0} \\ \frac{c_i}{d_i} - \frac{c_0}{d_0} \end{bmatrix} - \frac{\Delta d(\Delta \mathbf{t} + \mathbf{t}_0)}{d_i d_0} \right), \quad (7)$$

where

$$\begin{aligned} \Delta u &= u_i - u_0, \Delta v = v_i - v_0, \\ \Delta x &= \frac{x_i}{d_i} - \frac{x_0}{d_0}, \Delta y = \frac{y_i}{d_i} - \frac{y_0}{d_0} \\ \Delta d &= d_i - d_0, \Delta \mathbf{t} = \mathbf{t} - \mathbf{t}_0. \end{aligned}$$

Compared with the wide range and incompact distribution of  $\mathbf{t}$ , the optimization target  $\Delta \mathbf{t}$  is formulated in relative offset, which distributes in a narrow range between  $-r$  to  $r$ , and  $r$  is the radius of the object. Because the object shape is known and fixed, the distribution of  $\Delta \mathbf{t}$  is invariant and decoupled with the absolute positions of the object.

Establishing a stable reference point can make data distribution uniform and compact, helping the network to learn the 6D pose. Based on the input data, we select the XYD mean as the  $(x_0, y_0, d_0)$ , and then leverage the  $(x_0, y_0, d_0)$  to calculate  $(u_0, v_0)$  values of reference point following the projection equation. This generation strategy holds a stable reference point on the 2D image plane and makes the reference point as much as possible close to the origin of the object in 3D space. More comparisons of reference point design strategies are provided in our ablation study.

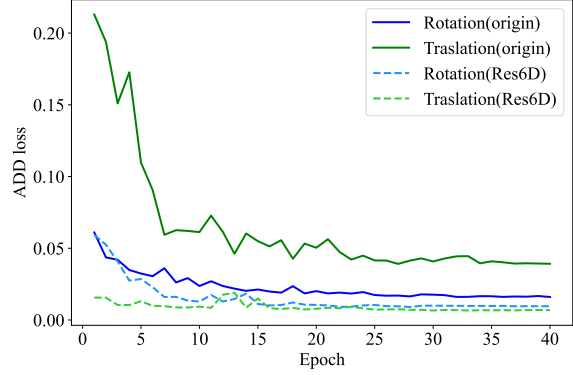


Figure 3. Balanced ADD loss on the Occlusion LineMOD dataset

### 3.3. Balanced ADD loss

To train the network to estimate 6D pose, ADD loss is a common choice for most methods. It heterogeneously transforms the points sampled on the object CAD model by the predicted poses and ground truth. It minimizes the distances of corresponding points between two different transformation points set. The specific loss is defined as

$$L_{ADD} = \frac{1}{m} \sum_j \|(\mathbf{R}x_j + \mathbf{t}) - (\hat{\mathbf{R}}x_j + \hat{\mathbf{t}})\|_2^2 \quad (8)$$

where  $x_j$  is the  $j^{th}$  point from  $m$  randomly sampled CAD model 3D points in the object coordinate system,  $(\mathbf{R}, \mathbf{t})$  is the predicted pose and  $(\hat{\mathbf{R}}, \hat{\mathbf{t}})$  is the ground truth pose. Re-combining Eq. (8), it can be reformulated as:

$$\begin{aligned} L_{ADD} &= \frac{1}{m} \sum_j \|(\Delta \mathbf{R}x_j + \Delta \mathbf{t})\|_2^2 \\ &= \frac{1}{m} \sum_j (\|\Delta \mathbf{R}x_j\|_2^2 + 2\Delta \mathbf{R}x_j \Delta \mathbf{t} + \|\Delta \mathbf{t}\|_2^2) \\ &= \frac{1}{m} \sum_j (\|\Delta \mathbf{R}x_j\|_2^2) + 2\Delta \mathbf{R} \sum_j x_j \Delta \mathbf{t} + \|\Delta \mathbf{t}\|_2^2 \end{aligned} \quad (9)$$

where  $\Delta \mathbf{R} = \mathbf{R} - \hat{\mathbf{R}}$ ,  $\Delta \mathbf{t} = \mathbf{t} - \hat{\mathbf{t}}$ . Since  $x_j$  is sampled from the object coordinate system, the centroid of sampled points is approx to the origin that  $\sum_j x_j \approx 0$ . Hence, the ADD loss is approximately equal to

$$L_{ADD} \approx \frac{1}{m} \sum_j (\|\Delta \mathbf{R}x_j\|_2^2) + \|\Delta \mathbf{t}\|_2^2 \quad (10)$$

which consists of the rotation part  $\frac{1}{m} \sum_j (\|\Delta \mathbf{R}x_j\|_2^2)$  and translation part  $\|\Delta \mathbf{t}\|_2^2$ . For the rotation part, since any point

on the object after rotating is inside the object’s circumscribed sphere, the rotation part is bounded by the object’s diameter. However, the translation part is unbounded because  $\mathbf{t}$  and  $\hat{\mathbf{t}}$  are absolute 3D translate vectors, denoting the centroid of the object in the camera frame, which can be any position in the 3D space. Hence, when  $\|\Delta\mathbf{t}\|_2^2 \gg 2 * r$ , the translation part obtains the optimization priority, and the rotation part will be neglected. The loss will be degraded to the  $l_2$  loss to fit the absolute value of the translation vector.

After adopting the reference point, the regression target translation vector is instead by an equivalent offset value between the object centroid and the reference point, which range is transformed into the range  $(-r, r)$  comparable to the rotation part. Therefore, the rotation and translation parts are balanced in the same magnitude. As shown in Fig. 3, the ADD loss has an obvious imbalance between the rotation and translation part, where the translation part occupies the majority. When leveraging the reference point, it pays equal attention to both rotation and translation transformations. Its’ translation part has a comparable loss to the rotation part. Hence, the rotation part is able to converge faster and the balanced loss shows better optimization results. The balanced ADD loss optimizes the regression network to find correspondences between input data and the CAD model transformed by rotation and the offset translate vector. Hence, the Res6D mechanism fixes the ADD loss degradation and simplifies the pose estimation task.

## 4. Experiments

### 4.1. Benchmark datasets

We conduct our experiments on four benchmark datasets.

**LineMOD** [13] contains 13 sequences of 13 low-textured objects. Since there is only about 1.2k real training data annotated with 6D pose, we follow previous work [12, 16, 21, 30] to add synthetic images for training with 99.71% synthetic ratio.

**Occlusion LineMOD** [1] consists of 1214 testing images that are selected from the LineMOD dataset in the occlusion scene. Since there is no extra real training data, the training dataset is the same as LineMOD. The domain gap between training and testing datasets, as well as the heavily occluded objects, make it more challenging for 6D pose estimation.

**YCB-Video** [2] is a large and challenging dataset that contains 21 objects with 92 RGB-D sequences. It provides a large amount of real training data holding the same pose distribution between training and testing datasets.

**T-LESS** [15] is an RGB-D dataset with 30 industry objects, which training data consists of individual objects with a black background but the test data is from real multiple instances scenes with occlusion and clutter. It exists signif-

icant location distribution and style gaps between training and testing datasets, which is challenging for methods to handle these domain gaps.

### 4.2. Evaluation metrics

We adopt the commonly used average distance metrics ADD, ADD-S, and ADD(S) to evaluate different methods. ADD evaluates the mean of pairwise distance between two object point clouds which are transformed according to the ground truth pose  $[\mathbf{R}, \mathbf{t}]$  and the predicted pose  $[\hat{\mathbf{R}}, \hat{\mathbf{t}}]$  respectively:

$$\text{ADD} = \frac{1}{m} \sum_{x \in \mathcal{O}} \|(\mathbf{R}x + \mathbf{t}) - (\hat{\mathbf{R}}x + \hat{\mathbf{t}})\| \quad (11)$$

where  $\mathcal{O}$  denotes the 3D model of a object,  $x$  denotes any point on the model and  $m$  denotes total point number in the model. To alleviate the ambiguous matching of the symmetric objects, ADD-S is adopted to estimate the closest point distance between two point clouds:

$$\text{ADD-S} = \frac{1}{m} \sum_{x_1 \in \mathcal{O}} \min_{x_2 \in \mathcal{O}} \|(\mathbf{R}x_1 + \mathbf{t}) - (\hat{\mathbf{R}}x_2 + \hat{\mathbf{t}})\|. \quad (12)$$

For convenience, we introduce ADD(S) metric:

$$\text{ADD(S)} = \begin{cases} \text{ADD} & \mathcal{O} \text{ is asymmetric} \\ \text{ADD-S} & \mathcal{O} \text{ is symmetric} \end{cases} \quad (13)$$

For LineMOD and Occlusion LineMOD datasets, we choose the threshold with 0.1d (10% of the diameter of the object) to calculate the accuracy of ADD(S), following [11, 21]. For the YCB-Video dataset and T-LESS dataset, following [11, 12, 20, 27, 30], we calculate the AUC (area under the accuracy-threshold curve) of ADD(S) with a maximum threshold of 0.1 meters.

### 4.3. Apply Res6D to different methods

To verify the extensibility of the proposed Res6D, we apply it to ES6D [20] and Uni6Dv2 [25]. These two methods have different frameworks, output targets, and loss functions.

**Apply Res6D mechanism to Uni6Dv2.** The input of Uni6Dv2 consists of an image patch  $(RGB, U, V, X, Y, D, NRM)$  which is cropped by the prediction of the segmentation network in the first stage. Then, the sparse regression network based on the image patch regresses the rotation and 3D location in the camera frame for each object and trains it through ADD Loss. To apply the Res6D mechanism to Uni6Dv2, we replace the visible points’ absolute positional encoding part  $(U, V, X, Y, D)$  with relative values  $(\Delta U, \Delta V, \Delta X, \Delta Y, \Delta D)$  between points to the reference point. The regression target is

	Res6D	Occlusion LineMOD	LineMOD	YCB-Video
Uni6Dv2	w/o	40.6	97.2	<b>91.5</b>
Uni6Dv2	w	<b>79.7(+39.1)</b>	<b>99.5(+2.3)</b>	<b>91.5</b>

Table 1. Evaluation results of Uni6Dv2 with Res6D on Occlusion LineMOD, LineMOD and YCB-Video datasets.

Setting	Res6D	YCB-Video	T-LESS
ES6D	w/o	89.0	93.1
ES6D	w	<b>95.4(+6.4)</b>	<b>99.1(+6.0)</b>

Table 2. Evaluation results of ES6D with Res6D on YCB-Video and T-LESS datasets.

reformulated as the offset of the reference point to the centroid. The comparison results are shown in Tab. 1. Since the 3D position variance of objects in Occlusion LineMOD is huge, after adopting the Res6D mechanism to convert into the offset encoding input, Uni6Dv2 shows an obvious improvement(+39.1%). More implementation details are provided in supplementary materials.

**Apply Res6D mechanism to ES6D.** The original ES6D feeds cropped RGB images with normalized  $(x, y, d)$  and leverages a dense regression network to predict the offsets of visible points to the centroid of an object and a confidence score. It introduces an A(M)GPD loss to replace the ADD loss to train the network. The final pose is selected by the point with the highest confidence score. To apply the Res6D mechanism to ES6D, the input is changed as  $(RGB, \Delta U, \Delta V, \Delta X, \Delta Y, \Delta D)$  based on the Eq. (7) and the regression target is changed as the residual regression target. Based on the comparison results in Tab. 2 using the Res6D mechanism holds the correspondences between RGB-D and CAD model, improving the performance of ES6D on YCB-Video(+6.4%) and T-LESS(+6.0%). More implementation details are provided in supplementary materials.

#### 4.4. Comparison with SOTA methods

We provide comprehensive and detailed comparison results on Occlusion LineMOD, LineMOD, and YCB-Video datasets. For the brevity of the paper, category-level experimental results on YCB-Video are provided in Supplementary Materials.

**Evaluation on Occlusion LineMOD dataset.** The quantitative results on the Occlusion LineMOD dataset are presented in Tab. 3. Compared with the baseline Uni6Dv2, employing the Res6D mechanism achieves a significant improvement (+39.1%) on ADD(S) metric and outperforms state-of-the-art method FFB6D [11](indirect method) by 13.5%. Noteworthy, adopting the Res6D mechanism makes

class	PoseCNN	PVN3D	FFB6D	Uni6D	Uni6Dv2	Ours
ape	9.6	33.9	47.2	33.0	44.3	63.0
can	45.2	88.6	85.2	51.1	53.3	90.9
cat	0.9	39.1	45.7	4.6	16.7	64.4
driller	41.4	78.4	81.4	58.4	63.0	83.3
duck	19.6	41.9	53.9	34.8	51.6	66.0
<b>eggbox</b>	22.0	80.9	70.2	1.7	4.6	90.9
<b>glue</b>	38.5	68.1	60.1	30.2	40.3	95.0
holepuncher	22.1	74.7	85.9	32.1	50.9	84.2
Avg	24.9	63.2	66.2	30.7	40.6	<b>79.7</b>

Table 3. Evaluation results on the Occlusion LineMOD dataset. Symmetric objects are denoted in bold. "Ours" is Uni6Dv2+Res6D.

	PoseCNN	DenseFusion	PVN3D	FFB6D	Uni6D	Uni6Dv2	Ours
ape	77.0	92.3	97.3	98.4	93.7	95.7	98.2
benchvise	97.5	93.2	99.7	100.0	99.8	99.9	100.0
camera	93.5	94.4	99.6	99.9	96.0	95.8	99.6
can	96.5	93.1	99.5	99.8	99.0	96.0	99.9
cat	82.1	96.5	99.8	99.9	98.1	99.2	99.1
driller	95.0	87.0	99.8	100.0	99.1	99.2	99.8
duck	77.7	92.3	97.7	98.4	90.0	92.1	97.4
<b>eggbox</b>	97.1	99.8	99.8	100.0	100.0	100.0	100.0
<b>glue</b>	99.4	100.0	100.0	100.0	99.2	99.6	100.0
holepuncher	52.8	92.1	99.9	99.8	90.2	92.0	99.7
iron	98.3	97.0	99.7	99.9	99.5	98.0	100.0
lamp	97.5	95.3	99.8	99.9	99.4	98.5	99.9
phone	87.7	92.8	99.5	99.7	97.4	97.7	99.8
Avg	88.6	94.3	99.4	<b>99.7</b>	97.0	97.2	99.5

Table 4. Evaluation results on the LineMOD dataset. Symmetric objects are denoted in bold. "Ours" is Uni6Dv2+Res6D

the network more reliable when there are significant translation distribution gaps.

**Evaluation on LineMOD dataset.** The quantitative results on the LineMOD dataset are presented in Tab. 4. Compared with our baseline Uni6Dv2, introducing the Res6D mechanism brings a 2.3% performance gain on ADD(S), demonstrating the effectiveness of our Res6D mechanism. Compared to FFB6D [11], the performance gap is minimal (99.5% vs. 99.7%), while our Res6D-based direct method has a more straightforward design and faster speed.

**Evaluation on YCB-Video dataset.** The quantitative results on the YCB-Video dataset are presented in Tab. 5. Compared with the baseline ES6D, introducing the Res6D mechanism brings a 6.4% performance gain on the AUC of ADD(S), demonstrating the effectiveness of our Res6D mechanism. Noteworthy, ES6D with Res6D mechanism outperforms the state-of-the-art method FFB6D [11] 2.7%.

In summary, our Res6D mechanism makes direct 6D pose estimation methods outperform indirect methods on Occlusion LineMOD and YCB-Video datasets, and achieve comparable accuracy on the LineMOD dataset.

#### 4.5. Reducing data dependency

In this section, we use fewer training data to explore the advantage of the Res6D mechanism, that is, it minimizes

	PoseCNN	DenseFusion	PVN3D	FFB6D	Uni6D	Uni6Dv2	ES6D	Uni6Dv2+Res6D	ES6D+Res6D
Avg	59.9	82.9	91.8	92.7	88.8	91.5	89.0	91.5	<b>95.4</b>

Table 5. Evaluation results on the YCB-Video dataset.

Training data ratio	Uni6Dv2		Uni6Dv2+Res6D	
	ADD-S	ADD(S)	ADD-S	ADD(S)
100%	96.8	91.5	96.6	91.5
10%	92.5	79.7	94.9	86.5
1%	79.1	57.1	91.9	76.6

Table 6. The advantage of reducing the amount of training data on the YCB-Video dataset.

Reference point generation strategies				ADD(S)
$u_0$ and $v_0$	$x_0$ and $y_0$	$d_0$		
ROI center	Projection values	nearest depth point		73.5
ROI center	Projection values	mean depth point		79.3
Projection values	mean of visible points	mean of visible points		<b>79.7</b>

Table 7. Comparison of generation strategies for the reference point ( $u_0, v_0, x_0, y_0, d_0$ ). ‘‘Projection values’’ can be calculated based on Eq. (6).

the translation distribution gap of the dataset to reduce the convergence difficulty of the network. We randomly sample 1% and 10% of the training data from YCB-Video as new training datasets. As listed in Tab. 6, compared with the baseline Uni6Dv2, the proposed method exhibits better performance on both 1% (57.1% vs. 76.6%) and 10% training data (79.7% vs. 86.5%) and has better robustness in case of reduced data volume. Especially, our method achieves comparable performance with full training data in ADD-S (94.9% vs. 96.6%) when only using 10% training data. Since YCB-Video has a large amount of real training data with the same pose distribution of test data, there is no obvious performance gain on 100% training data. The main reason of the Res6D mechanism reducing data dependency is that it narrows the translation distribution gap between the training and testing datasets, easing the network regression learning. It is meaningful for practical 6D pose estimation applications where data collection and labeling are expensive.

#### 4.6. Ablation study

In this section, we will analyze the effectiveness of the Res6D mechanism and compare different reference point generation strategies on Uni6Dv2. All experiments are conducted on the Occlusion LineMOD dataset.

**Effect and efficiency of Res6D mechanism.** We analyze the effect of different residual regression strategies, in-

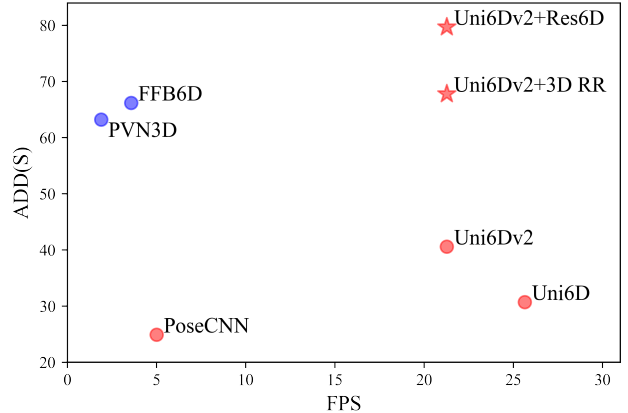


Figure 4. Comparison of speed and accuracy on the Occlusion LineMOD: Uni6Dv2+Res6D achieves state-of-the-art accuracy in both direct regression methods (red dots) and indirect regression methods (blue dots) methods. 3D RR denotes the 3D residual regression mechanism.

cluding the 3D residual regression and the projective residual regression. When introducing the naive 3D residual regression into Uni6Dv2, it selects a visible point from the  $XYD$  value to convert the absolute 3D coordinate in the input data and output target into a relative value. After leveraging the 3D residual regression, the performance of Uni6Dv2 improves by 27.2%, achieving 67.8% w.r.t ACC-ADD(S). Meanwhile, due to the mismatch problem in Eq. (2) and Eq. (3), it still has room to improve. When adopting the projective residual regression, there is an obvious performance gain from 40.6% to 79.7%, and it shows an 11.9% advanced improvement compared with the 3D residual regression version. Moreover, for analyzing efficiency, as shown in Fig. 4, the projective residual regression merely does not introduce extra time consumption and helps Uni6Dv2 outperform the current SOTA RGB-D method FFB6D [11] 13.5% while 5.6 times faster than it. The improvement demonstrates that the projective residual regression alleviates the translation distribution gap and optimizes the network to learn pose estimation.

**Reference point generation strategies.** To build a stable reference point, we attempt three different reference point generation strategies, as shown in Tab. 7. The first strategy selects the UV value ( $u_0, v_0$ ) of the ROI region center, the nearest point’s depth as reference point depth, and

then calculates  $x_0$  and  $y_0$  based on Eq. (6). The ROI center as the reference point in the 2D image plane maintains a stable UV encoding and attempts to use the center point’s depth to project the reference point in the 3D space. However, since the center point in ROI is likely in the outside or margin of the object due to the occlusion or the irregular, the depth value may be lost or a noise point from the sensor. To alleviate this problem, the second strategy adopts the mean depth value of the object region as the reference depth, which improves the stability of the Res6D mechanism in the 2D image plane and 3D space, achieving a 5.8% improvement from 73.5% to 79.3%. Besides the reference point selection based on the UV, the third strategy adopts the mean XYD of visible points as the reference point and calculates the  $(u_0, v_0)$  through the Eq. (6). Compared with the selection from UV, it is prone to consider the 3D shape and shows similar performance to the UV selection strategy. Hence, whatever the reference point generation considers the 2D shape or 3D shape, the Res6D mechanism can demonstrate its effectiveness.

#### 4.7. Visualization

Visualization results of the Occlusion LineMOD dataset are shown in Fig. 5. We can observe that Uni6Dv2+Res6D could predict a more precise and robust 6D pose on the heavily occluded objects compared to other methods. Moreover, benefiting from the Res6D mechanism, the orientation of objects with only a few visible points is correctly predicted, which proves that the proposed Res6D mechanism improves the robustness and generalization of the network.

### 5. Limitations and discussion

**Choosing reference point** The current Res6D reference point generation strategy follows the prior that the mean point is close to most objects’ centroid. However, the mean point of irregular objects is likely far away from the centroid, which hardly builds a corresponding stable reference point on the CAD model. Although the clustering methods [4] can find a closer point, the cluster iteration introduces extra computing consumption, limiting the efficiency.

**Apply Res6D mechanism to indirect methods** Indirect methods such as PVN3D [12] and FFB6D [11] adopt the dense prediction framework to fit the intermediate geometric information, *e.g.* keypoints. Based on the dense prediction network, it leverages each pixel as a reference point and regresses the offset value between keypoints. The offset regression target is not the final pose, limiting the Res6D mechanism based on the residual-based projection model to learn the correspondence between the CAD model and current input data.

**Distribution of residual** As we can see in Figure 1a, no matter what the distribution of original  $t, X, Y, D$  is, their residuals approximate to a standard Gaussian distribution

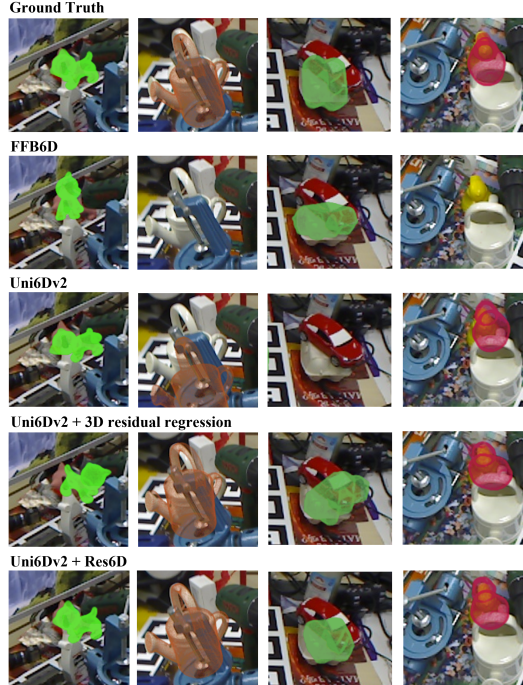


Figure 5. Qualitative results of 6D pose estimation on the Occlusion LineMOD dataset.

based on central limit theorem, whose mean is close to 0 and variance in a much smaller range. This new distribution avoids issues related to over-parametrization and makes the target value easy to learn for the CNN network.

### 6. Conclusion

In this paper, we present the benefits of introducing the projective residual regression (Res6D) mechanism in 6D pose estimation, *i.e.*, alleviating the conflict of data variance and CNN channel equilibrium, and uncovering the mismatch issue about the 3D reference regression mechanism in 6D pose regression tasks. A residual-based projection model is derived from the projection equation, and the Res6D mechanism with reference point is naturally proposed. Various reference point generation strategies are evaluated, and the optimal one is applied to different direct regression methods, such as Uni6Dv2 and ES6D. Experiments demonstrate that applying the Res6D mechanism to direct regression methods, achieves state-of-the-art Occlusion LineMOD and YCB-Video datasets. Furthermore, the proposed method greatly reduces the demand for training data, which is crucial in practice.

We believe that the Res6D mechanism is able to inspire other 3D tasks, such as category-level pose estimation, 3D reconstruction, 3D object detection with RGB-D or Lidar data, since the underlying data input of these 3D tasks inherently, follows projection constraints.



## References

- [1] Eric Brachmann, Alexander Krull, Frank Michel, Stefan Gumhold, Jamie Shotton, and Carsten Rother. Learning 6d object pose estimation using 3d object coordinates. In *European conference on computer vision*, pages 536–551, 2014. [2](#), [5](#)
- [2] Berk Calli, Arjun Singh, Aaron Walsman, Siddhartha Srinivasa, Pieter Abbeel, and Aaron M Dollar. The ycb object and model set: Towards common benchmarks for manipulation research. In *2015 international conference on advanced robotics (ICAR)*, pages 510–517, 2015. [5](#)
- [3] Xiaozhi Chen, Huimin Ma, Ji Wan, Bo Li, and Tian Xia. Multi-view 3d object detection network for autonomous driving. In *Proceedings of the IEEE conference on Computer Vision and Pattern Recognition*, pages 1907–1915, 2017. [1](#)
- [4] Yizong Cheng. Mean shift, mode seeking, and clustering. *IEEE transactions on pattern analysis and machine intelligence*, 17(8):790–799, 1995. [8](#)
- [5] Zijun Deng, Xiaowei Hu, Lei Zhu, Xuemiao Xu, Jing Qin, Guoqiang Han, and Pheng-Ann Heng. R3net: Recurrent residual refinement network for saliency detection. In *Proceedings of the 27th International Joint Conference on Artificial Intelligence*, pages 684–690. AAAI Press Menlo Park, CA, USA, 2018. [3](#)
- [6] Yixin Du and Xin Li. Recursive deep residual learning for single image dehazing. In *Proceedings of the IEEE Conference on Computer Vision and Pattern Recognition Workshops*, pages 730–737, 2018. [3](#)
- [7] Max Ehrlich and Larry S Davis. Deep residual learning in the jpeg transform domain. In *Proceedings of the IEEE/CVF International Conference on Computer Vision*, pages 3484–3493, 2019. [3](#)
- [8] Andreas Geiger, Philip Lenz, and Raquel Urtasun. Are we ready for autonomous driving? the kitti vision benchmark suite. In *2012 IEEE conference on computer vision and pattern recognition*, pages 3354–3361, 2012. [1](#)
- [9] Rasmus Laurvig Haugaard and Anders Glent Buch. Surfem: Dense and continuous correspondence distributions for object pose estimation with learnt surface embeddings. In *Proceedings of the IEEE/CVF Conference on Computer Vision and Pattern Recognition*, pages 6749–6758, 2022. [1](#), [3](#)
- [10] Kaiming He, Xiangyu Zhang, Shaoqing Ren, and Jian Sun. Deep residual learning for image recognition. In *Proceedings of the IEEE conference on computer vision and pattern recognition*, pages 770–778, 2016. [3](#)
- [11] Yisheng He, Haibin Huang, Haoqiang Fan, Qifeng Chen, and Jian Sun. Ffb6d: A full flow bidirectional fusion network for 6d pose estimation. In *Proceedings of the IEEE/CVF Conference on Computer Vision and Pattern Recognition*, pages 3003–3013, 2021. [1](#), [2](#), [3](#), [5](#), [6](#), [7](#), [8](#)
- [12] Yisheng He, Wei Sun, Haibin Huang, Jianran Liu, Haoqiang Fan, and Jian Sun. Pvn3d: A deep point-wise 3d keypoints voting network for 6dof pose estimation. In *Proceedings of the IEEE/CVF conference on computer vision and pattern recognition*, pages 11632–11641, 2020. [1](#), [2](#), [3](#), [5](#), [8](#)
- [13] Stefan Hinterstoisser, Stefan Holzer, Cedric Cagniart, Slobodan Ilic, Kurt Konolige, Nassir Navab, and Vincent Lepetit. Multimodal templates for real-time detection of texture-less objects in heavily cluttered scenes. In *2011 international conference on computer vision*, pages 858–865, 2011. [5](#)
- [14] Tomas Hodan, Daniel Barath, and Jiri Matas. Epos: Estimating 6d pose of objects with symmetries. In *Proceedings of the IEEE/CVF conference on computer vision and pattern recognition*, pages 11703–11712, 2020. [3](#)
- [15] Tomáš Hodan, Štěpán Obdržálek, Jiri Matas, Manolis Lourakis, and Xenophon Zabulis. T-less: An rgb-d dataset for 6d pose estimation of texture-less objects. In *2017 IEEE Winter Conference on Applications of Computer Vision (WACV)*, pages 880–888. IEEE, 2017. [5](#)
- [16] Xiaoke Jiang, Donghai Li, Hao Chen, Ye Zheng, Rui Zhao, and Liwei Wu. Uni6d: A unified cnn framework without projection breakdown for 6d pose estimation. *IEEE/CVF Conference on Computer Vision and Pattern Recognition (CVPR)*, 2022. [1](#), [3](#), [5](#)
- [17] P Kiru, Timothy Patten, and MV Pix2Pose. Pixel-wise coordinate regression of objects for 6d pose estimation. *Proceedings of the ICCV, Seoul, Korea*, pages 27–28, 2019. [1](#), [3](#)
- [18] Yi Li, Gu Wang, Xiangyang Ji, Yu Xiang, and Dieter Fox. Deepim: Deep iterative matching for 6d pose estimation. In *Proceedings of the European Conference on Computer Vision (ECCV)*, pages 683–698, 2018. [1](#), [3](#)
- [19] Zhigang Li, Gu Wang, and Xiangyang Ji. Cdpn: Coordinates-based disentangled pose network for real-time rgb-based 6-dof object pose estimation. In *Proceedings of the IEEE/CVF International Conference on Computer Vision*, pages 7678–7687, 2019. [1](#), [3](#)
- [20] Ningkai Mo, Wanshui Gan, Naoto Yokoya, and Shifeng Chen. Es6d: A computation efficient and symmetry-aware 6d pose regression framework. In *Proceedings of the IEEE/CVF Conference on Computer Vision and Pattern Recognition*, pages 6718–6727, 2022. [1](#), [3](#), [5](#)
- [21] Sida Peng, Yuan Liu, Qixing Huang, Xiaowei Zhou, and Hujun Bao. Pvnnet: Pixel-wise voting network for 6dof pose estimation. In *Proceedings of the IEEE/CVF Conference on Computer Vision and Pattern Recognition*, pages 4561–4570, 2019. [2](#), [5](#)
- [22] Mahdi Rad and Vincent Lepetit. Bb8: A scalable, accurate, robust to partial occlusion method for predicting the 3d poses of challenging objects without using depth. In *Proceedings of the IEEE international conference on computer vision*, pages 3828–3836, 2017. [1](#), [3](#)
- [23] Xibin Song, Yuchao Dai, Dingfu Zhou, Liu Liu, Wei Li, Hongdong Li, and Ruigang Yang. Channel attention based iterative residual learning for depth map super-resolution. In *Proceedings of the IEEE/CVF Conference on Computer Vision and Pattern Recognition*, pages 5631–5640, 2020. [3](#)
- [24] Yongzhi Su, Mahdi Saleh, Torben Fetzner, Jason Rambach, Nassir Navab, Benjamin Busam, Didier Stricker, and Federico Tombari. Zebrapose: Coarse to fine surface encoding for 6dof object pose estimation. In *Proceedings of the IEEE/CVF Conference on Computer Vision and Pattern Recognition*, pages 6738–6748, 2022. [1](#), [3](#)

- [25] Mingshan Sun, Ye Zheng, Tianpeng Bao, Jianqiu Chen, Guoqiang Jin, Rui Zhao, Liwei Wu, and Xiaoke Jiang. Uni6dv2: Noise elimination for 6d pose estimation. *arXiv preprint arXiv:2208.06416*, 2022. [1](#), [3](#), [5](#)
- [26] Jia Wan, Wenhan Luo, Baoyuan Wu, Antoni B Chan, and Wei Liu. Residual regression with semantic prior for crowd counting. In *Proceedings of the IEEE/CVF Conference on Computer Vision and Pattern Recognition*, pages 4036–4045, 2019. [3](#)
- [27] Chen Wang, Danfei Xu, Yuke Zhu, Roberto Martín-Martín, Cewu Lu, Li Fei-Fei, and Silvio Savarese. Densefusion: 6d object pose estimation by iterative dense fusion. In *Proceedings of the IEEE/CVF conference on computer vision and pattern recognition*, pages 3343–3352, 2019. [1](#), [3](#), [5](#)
- [28] Gu Wang, Fabian Manhardt, Jianzhun Shao, Xiangyang Ji, Nassir Navab, and Federico Tombari. Self6d: Self-supervised monocular 6d object pose estimation. In *European Conference on Computer Vision*, pages 108–125. Springer, 2020. [1](#), [3](#)
- [29] Gu Wang, Fabian Manhardt, Federico Tombari, and Xiangyang Ji. Gdr-net: Geometry-guided direct regression network for monocular 6d object pose estimation. In *Proceedings of the IEEE/CVF Conference on Computer Vision and Pattern Recognition*, pages 16611–16621, 2021. [1](#), [3](#)
- [30] Yu Xiang, Tanner Schmidt, Venkatraman Narayanan, and Dieter Fox. Posecnn: A convolutional neural network for 6d object pose estimation in cluttered scenes. In *Robotics: Science and Systems (RSS)*, 2018. [5](#)
- [31] Danfei Xu, Dragomir Anguelov, and Ashesh Jain. Pointfusion: Deep sensor fusion for 3d bounding box estimation. In *Proceedings of the IEEE conference on computer vision and pattern recognition*, pages 244–253, 2018. [1](#)